Synthesis of $CsPbBr_3$ Quantum Dots for Photodetectors

Zizhao Xu

A thesis

submitted in partial fulfillment of the

requirements for the degree of

Master of Science

University of Washington

2020

Committee:

Qiuming Yu

René Overney

Program Authorized to Offer Degree:

Chemical Engineering

University of Washington

Abstract

Synthesis of $CsPbBr_3$ Quantum Dots for Photodetectors

Zizhao Xu

Chair of the Supervisory Committee:
Professor Qiuming Yu
Department of Chemical Engineering

Metal halide perovskites (MHP) represent a flourishing area of research, which is driven by both their potential applications in photovoltaics and optoelectronics and by the fundamental science behind their unique optoelectronic properties. we synthesized $CsPbBr_3$ quantum dots (QDs) via the LARP method at RT and mixed them with conjugate polymer to fabricate nanocomposite photodetectors. We found that the size and optical properties of $CsPbBr_3$ QDs are affected by varying the amount of precursor injected into antisolvent, ligands in precursor or antisolvent, and centrifugation speed. Besides, we have fabricated the conventional sandwich structure photodiode by using $CsPbBr_3$ QDs blended with conjugated polymer Poly[(9,9-dioctylfluorenyl-2,7-diyl)-alt-co-(bithiophene)] F8T2 as the active layer. The dark current might depend on the weight ratio of F8T2:$CsPbBr_3$ and the structure of device, which we will focus on in the future.

TABLE OF CONTENTS

LIST OF FIGURES

LIST OF TABLES

ACKNOWLEDGEMENTS

I want to express my sincere appreciation to my advisor Professor Qiuming Yu to her guidance and encouragement, Professor René Overney as my committee, my group members Dr. Monica Esopi, Gabriella Tosado, Erjin Zheng, Xiaoyu Zhang, Emerson Chen, Hao Dong, Zonglun Li, Zhiyin Niu, Wenxin Cao and Shukun Zhong for their ideas, and my parents and friends for their invaluable support.

Chapter 1. INTRODUCTION

Metal halide perovskites (MHP) represent a flourishing area of research, which is driven by both their potential applications in photovoltaics and optoelectronics and by the fundamental science behind their unique optoelectronic properties. Although metal halide perovskites were first reported in 1893, it was not until 1990s that they began to attract the attention of the scientific and engineering community.[1] New colloidal methods for the synthesis of metal halide perovskite nanocrystals (MHP NCs), as well as the optical properties of this new type of material, has attracted the attention of many researchers.[2]

In order to prepare high quality MHP NCs in terms of having control over the size, shape and quality of their optical properties, two most developed liquid-phase methods have been used to synthesize colloidal MHP NCs: the hot injection method and ligand-assisted reprecipitation (LARP) method.[3] Compared with hot injection method, the LARP method can be employed as a more cost-effective alternative, as it delivers high quality perovskite NCs in an ambient atmosphere at room temperature (RT).[4] The LARP method, when applied to perovskite systems, simply consists of dropping the desired precursor salts, dissolved in a good polar solvent, such as dimethylformamide (DMF), into a poor solvent such as toluene with the help of ligands. In other words, The mixture of the two solvents induces an instantaneous supersaturation, which triggers the nucleation and the growth of perovskite NCs.[2] The first reports on LARP syntheses of hybrid organic-inorganic lead halide based perovskite NCs date back to 2012 when Papavassiliou *et al*. synthesized the methylammonium lead trihalide（$MAPbX_3$）and observed the formation of luminescent NCs.[5] Until 2015, all-inorganic $CsPbX_3$ NCs (where X = I^-, Br^-, and Cl^-) could only be synthesized using the hot-injection approach.[6] In 2016, Li *et al.* showed that all-inorganic

perovskite systems in the form of colloidal NCs could also be produced using the LARP approach at RT. They used the CsX rather than MAX in the precursor solution and observed the formation of $CsPbX_3$.[7] Seth *et al.* further optimized the LARP method to achieve control over the morphology of $CsPbX_3$.[8] They reported the shape of the NCs could be controlled by varying the bad solvent, the relative amount of ligands, and the reaction time. Besides, they found the concentration of oleylamine (OLA) is high enough in toluene, the NC surfaces become more protected in all directions, which consequently prevents both attachment/merging and growth of NCs. Using ethyl acetate as the nonpolar solvent, instead of toluene , causes more OLA molecules to detach themselves from the surface of the growing nuclei because ethyl acetate is more polar than toluene and can act both as a solvent and a nucleophile.[8]

With the development of colloidal synthesis methods, high quality MHP NCs are prepared and applied in more fields such as phototransistors, photodiodes and so on. Inorganic halide perovskite-based photodetectors have exhibited fast response speed and high responsivity. Zeng *et al.* have reported the method to control dark current. As a result, the photo-/dark-current ratio reaches a giant value of 2.13×10^8, and the peak detectivity is as high as 1.24×10^{13} Jones by using poly(methyl methacrylate) (PMMA) as the tunneling organic layer to solve the instability of MHP NCs and interface deterioration.[9]

In this work, we synthesized $CsPbBr_3$ quantum dots (QDs) via the LARP method at RT and mixed them with conjugate polymer to fabricate nanocomposite photodetectors. We found that the size and optical properties of $CsPbBr_3$ QDs are affected by varying the amount of precursor injected into antisolvent, ligands in precursor or antisolvent, and centrifugation speed. Besides, we have fabricated the conventional sandwich structure photodiode by using $CsPbBr_3$ QDs blended with conjugated polymer Poly[(9,9-dioctylfluorenyl-2,7-diyl)-alt-co-(bithiophene)] F8T2 as the

active layer. To investigate the performance of device, we tested the dark current and photocurrent of the device. Although all fabricated devices were unstable, the appropriate weight ratio of F8T2:$CsPbBr_3$ QDs and improved device structure could be the future work.

Chapter 2. EXPERIMENT

2.1 Materials

Materials: ITO-coated glass (≤10 Ω sq−1) was purchased from Colorado Concept Coatings LLC. Poly[(9,9-dioctylfluorenyl-2,7-diyl)-alt-co-(bithiophene)] (F8T2) was purchased from American Dye Source (Baie D'Urfe, Quebec, Canada, 30000 g/mol and polydispersity indexes of 4.5), Poly(3,4-ethylenedioxythiophene)-poly(styrenesulfonate) (PEDOT:PSS) solution (Clevios P VP AI 4083) was purchased from Heraeus (Hanau, Germany). Poly[[4,8-bis[(2-ethylhexyl)oxy]benzo[1,2-b:4,5-b']dithiophene-2,6-diyl][3-fluoro-2-[(2 ethylhexyl)carbonyl]thieno[3,4-b]thiophenediyl]] (PTB7) and Poly([2,6′-4,8-di(5-ethylhexylthienyl)benzo[1,2-b;3,3-b]dithiophene]{3-fluoro-2[(2-ethylhexyl)carbonyl]thieno[3,4-b]thiophenediyl}) (PTB7-Th) were purchased from 1-Material (Dorval, Quebec, Canada). CsBr (99.999%), $PbBr_2$ (99.999%), oleic acid (OA, ≥99%), oleylamine (OLA, 70%), N,N-Dimethylformamide (DMF, 99.9%), toluene (99.8%), acetonitrile (99.8%), 2,9-dimethyl-4,7-diphenyl-1,10 phenanthroline (BCP, 99.99%), and lithium fluoride (LiF, 99.995%) were purchased from Sigma-Aldrich. Aluminum pellets of 99.999% purity were purchased from R. D. Mathis.

2.2 $CsPbBr_3$ quantum dots synthesis

Colloidal perovskite $CsPbBr_3$ QDs were synthesized by the LARP method.[10] Oleic acid and oleylamine were used as ligands and they were added in the anti-solvent or the precursor solution.

In a typical synthesis with the ligands in the anti-solvent, a mixture of 0.016 mmol CsBr and 0.0245 mmol $PbBr_2$ was dissolved in 0.5 mL of DMF via ultrasonication. A 0.25 mL of precursor solution was added to 10 mL of toluene with 0.05 mL of oleic acid and 0.005 mL oleylamine under vigorous stirring. A bright yellow solution was immediately observed. After centrifugation at 12000 rpm for 10 min using Fluorinated ethylene propylene (FEP) centrifuge tubes to discard the precipitates, a bright blue-green colloidal solution was obtained. Other synthesis conditions are listed in Table 2.1.

Table 2. 1. Synthesis of $CsPbBr_3$ QDs with ligands in anti-solvent under different conditions. The QD concentration was calculated based on the complete reaction with the reactants.

Batch	Precursor (mmol/mL)	Inject Volume (mL)	Anti-solvent (mL)	Centrifuge Speed (rpm)	QD Concentration (mmol/mL)
1	CsBr: 0.032 $PbBr_2$: 0.049	0.25	OA: 0.05 OLA: 0.005 Toluene: 10	12000	0.0008
2	CsBr: 0.032 PbBr2: 0.049	1	OA: 0.05 OLA: 0.005 Toluene: 10	12000	0.0032
3	CsBr: 0.032 $PbBr_2$: 0.049	0.25	OA: 0.05 OLA: 0.005 Toluene: 10	7000	0.0008
4	CsBr: 0.032 $PbBr_2$: 0.049	0.25	OA: 0.05 OLA: 0.005 Toluene: 10	4000	0.0008

In a typical synthesis with the ligands in the precursor solution, a mixture of 0.064 mmol CsBr and 0.098 mmol $PbBr_2$ was dissolved in 2 mL of DMF via ultrasonication. 0.08 mL of oleic acid and 0.04 mL oleylamine were added in 0.88 mL of the precursor solution, which was added into 10 mL of toluene under vigorous stirring. A bright green solution was immediately observed. After centrifugation at 12000 rpm for 10 min using Fluorinated ethylene propylene (FEP) centrifuge tubes to discard the precipitates, a bright blue-green colloidal solution was obtained. Other

synthesis conditions are listed in Table 2.2.

Table 2. 2. Synthesis of $CsPbBr_3$ QDs with ligands in the precursor solution under different conditions. The QD concentration was calculated based on the complete reaction with the reactants.

Batch	Precursor (mmol/mL)	Inject Volume (mL)	Anti-solvent Toluene (mL)	Centrifuge Speed (rpm)	QD Concentration (mmol/mL)
5	CsBr:0.032 $PbBr_2$:0.049	Precursor:0.88 OA:0.08 OLA:0.04	10	12000	0.0032
6	CsBr: 0.032 $PbBr_2$: 0.049	Precursor:0.25 OA:0.05 OLA:0.005	10	4000	0.008
7	CsBr: 0.032 $PbBr_2$: 0.049	Precursor:1 OA:0.2 OLA:0.02	10	4000	0.0032
8	CsBr:0.032 $PbBr_2$:0.049	Precursor:2 OA:0.4 OLA: 0.04	10	4000	0.0064

In order to synthesize $CsPbBr_3$ QDs directly in the conjugated polymer solution, we dissolved PTB7 or PTB7-Th in toluene and used it as “anti-solvent”. A dark-purple solution was observed for the pure PTB7 or PTB7-Th toluene solution. In a typical synthesis, a mixture of 0.016 mmol CsBr and 0.0245 mmol $PbBr_2$ was dissolved in 0.5 mL of DMF via ultrasonication. A 0.25 mL of the precursor solution was added to 10 mL of PTB7 solution (0.4 mg/mL in toluene) under vigorous stirring. After centrifugation at 12000 rpm for 10 min to discard the precipitates, a dark-purple colloidal solution was obtained. Other synthesis conditions are listed in Table 2.3.

Table 2. 3. Synthesis of $CsPbBr_3$ QDs with PTB7 and PTB7-Th in toluene as anti-solvent under different conditions. The QD concentration is calculated based on the complete reaction with the reactants.

Batch	Precursor (mmol/mL)	Inject Volume (mL)	Anti-solvent	Centrifuge speed (rpm)	QD Concentration (mmol/mL)
9	CsBr: 0.032 $PbBr_2$: 0.049	0.25	PTB7: 0.4 mg/mL Toluene: 10 mL	12000	0.0008
10	CsBr: 0.032 $PbBr_2$: 0.049	0.25	PTB7-Th: 0.4 mg/mL Toluene: 10 mL	12000	0.0008

In order to concentrate the supernatant, typically, 4 mL bright blue-green supernatant solution was added to a new FEP centrifuge tube and mixed with 4 mL acetonitrile. Ten minutes later, the precipitates were observed. After the mixed solution stood for about 30 min at room temperature, the mixed solution was centrifuged at 4000 rpm for 10 min. Following the centrifugation, the supernatant was discarded, and the precipitate was re-dispersed in 1 mL toluene to get the concentrated $CsPbBr_3$ QDs. The concentration of the concentrated $CsPbBr_3$ QDs was doubled compared with that of the original supernatant estimated by the UV-Vis absorption spectra.

2.3 Fabrication of $CsPbBr_3$ QDs and F8T2 films and photodetectors

Plain glass slides were cut by 15 mm x 15 mm and cleaned by ultrasonication for 15 min each in soapy deionized (DI) water, DI water, acetone, and isopropyl alcohol (IPA), in sequence, and then by oxygen plasma cleaning at 100 W for 30 s. The polymer F8T2 was dissolved separately in toluene (25 mg/mL) and stirred at 700 rpm and 70 °C for at least 12 h. The $CsPbBr_3$ was dispersed in toluene with different concentrations at room temperature in glovebox. These individual solutions were then combined in varying F8T2:$CsPbBr_3$ weight ratios including 5:1, 10:1, 100:4,

1:3 and 1:6. The F8T2:$CsPbBr_3$ blend precursor solutions were filtered through a 0.2 μm polytetrafluoroethylene (PTFE) syringe filter and deposited via spin coating at 1000 rpm (unless otherwise stated) for 30 s. The films were then annealed at 80°C for 10 min. All film fabrication steps, after the preparation of the substrates, were completed in a nitrogen-filled glovebox. Film analysis was performed in ambient conditions.

To fabricate photodetectors, ITO coated glass substrates (15 mm x 15 mm) were prepared as the glass substrates used for film fabrication. PEDOT:PSS solution was filtered through a 0.45 μm nylon syringe filter and spin-coated on the cleaned ITO-coated glass substrates at 3000 rpm for 60 s, then baked at 120 °C for 30 min in air. The chips were then transferred into a nitrogen-filled glovebox (O_2 and H_2O levels <5 ppm). The F8T2:$CsPbBr_3$ QD active layers were deposited via spin coating, under the same conditions as the previously described F8T2:$CsPbBr_3$ QD films. A thin 0.8 nm layer of LiF was deposited via thermal evaporation, without the use of any mask. Or a layer of BCP (dissolved in isopropanol, 10 mg/mL) was deposited via spin coating at 4000 rpm for 60 s. Finally, 100 nm aluminum electrodes were then deposited via thermal evaporation with rectangular masks so that the active area of each device was 0.1 cm^2.

2.4 Characterization

2.4.1 $CsPbBr_3$ QDs characterization

UV-vis and photoluminescence (PL) spectra were collected using a Varian Cary 5000 UV-vis spectrophotometer and a Horiba Fluorolog 3 spectrofluorometer, respectively. Transmission electron microscopy (TEM) images were collected with a Tecnai G2 F20 Supertwin TEM.

2.4.2 Film and device characterization

Film analysis was performed in ambient conditions. UV–vis and PL spectra of thin films were collected using the same instruments mentioned above. Film thicknesses were measured using a Bruker DektakXT profilometer. AFM images were collected with a Digital Instrument Multimode AFM. All device characterizations were performed in air. Current density versus voltage (*J–V*) curves, were obtained using a Keithley 2635B sourcemeter. Unless otherwise noted, scan direction was from forward bias to reverse bias (-5 to +5 V or -3 to +3 V). Light was provided using a Xenon arc lamp and an Oriel Cornerstone 130 Monochromator, and optical intensity was measured using a Newport 1918-R Power Meter and Newport UV-Si Photodiode.

Chapter 3. RESULTS AND DISCUSSION

3.1 Synthesis of $CsPbBr_3$ QDs with ligands in anti-solvent

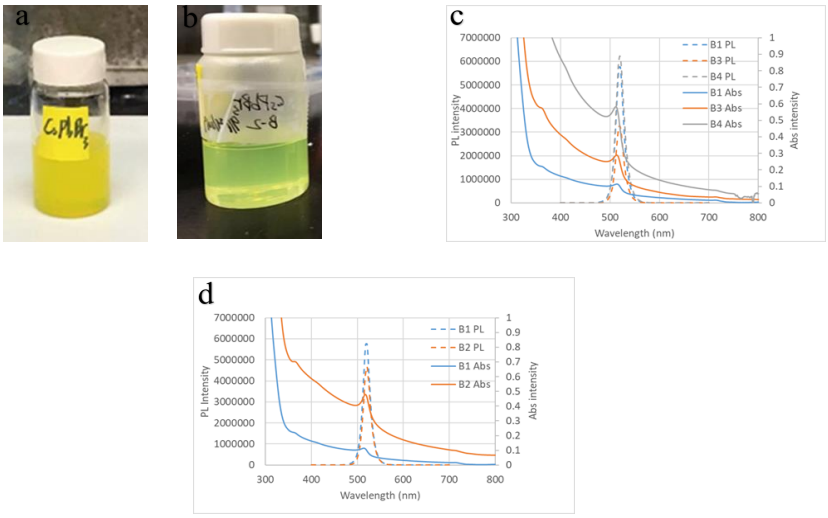

Figure 3.1. Photographs of (a) as synthesized and (b) supernatant of B1 $CsPbBr_3$ QDs. (c) UV-Vis absorption and PL spectra of B1, B3 and B4 $CsPbBr_3$ QDs. (d) UV-Vis absorption and PL spectra of B1 and B2 $CsPbBr_3$ QDs. PL was excited by a 365 nm light.

We adopted the LARP method[10] with some modifications to synthesize $CsPbBr_3$ QDs. Briefly,

the precursor solution was prepared by dissolving the appropriate amount of $PbBr_2$ and CsBr in polar solvent DMF. The appropriate amount of OA and OLA ligands was added in non-polar toluene anti-solvent. Colloidal $CsPbBr_3$ QDs were formed when the precursor solution was added into a poor solvent for perovskite under vigorous stirring at room temperature. After atoms nucleated and grew by diffusion or reaction about 30 min,[11] we obtained a crude yellow $CsPbBr_3$ colloid solution as shown in Figure 3.1a. $CsPbBr_3$ QDs were further separated from the crude solution by centrifugation. After centrifuge using FEP centrifuge tubes at 12000 rpm for 10 min at room temperature, we collected the bright yellow green supernatant as shown in Figure 3.1b. We prepared three batches of $CsPbBr_3$ QDs under the same reaction condition but different centrifugation speeds, and characterized them via UV-Vis and PL spectrometers. As shown in Figure 3.1c, the UV-Vis spectrum of each batch has an absorption edge around 515 nm and the UV-Vis intensity of $CsPbBr_3$ supernatant decreases with the increasing centrifugation speed, implying that the centrifugation speed has no influence on the size of synthesized $CsPbBr_3$ QDs but the concentration of $CsPbBr_3$ QDs in supernatant decreases. PL spectra of all batches exhibit the sharp emission peaks in the range of 519-523 nm, indicating a slight change of the particle size. The observed Stokes shifts is an obvious excitonic feature implying that the PL emission originates from excitonic recombination.[12] Figure 3.1d shows the evolution of $CsPbBr_3$ QD absorption and PL with different injected volumes of the precursor solution while keeping the same other experimental conditions. The increase of injected volume of the precursor solution results in an increase of UV-Vis intensity and a decrease of PL intensity. The strong increase of UV-Vis intensity can be attributed to the growth of much more nuclei to nanocrystals with increasing amount of precursor. The slight decrease of PL intensity implies more nuclei or atoms in the $CsPbBr_3$ QDs solution which can feed the growth of larger $CsPbBr_3$ QDs, or the coalescence of the QDs. These

mechanisms would lead to more mono-dispersed population of larger particles and they would create more defects, which make non-radiative recombination more probable, thereby decreasing the PL intensity.[13] These mechanisms also explain the slight reduced bandgap, which is expressed by narrowing and red shift of the QD emission line from 519 to 521 nm as shown in Figure 3.1d.

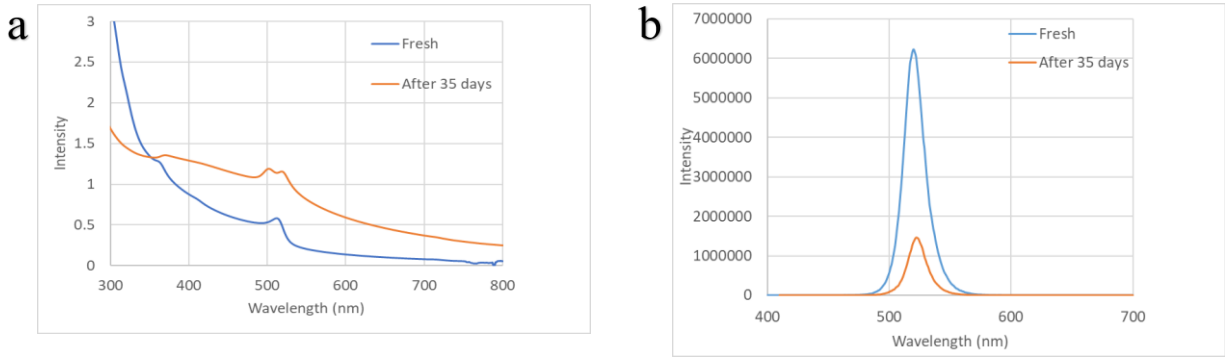

Figure 3.2. (a) UV-Vis absorption spectra and (b) PL spectra of fresh B4 and B4 stored in a nitrogen glovebox for 35 days. The excitation wavelength is 365 nm for PL.

As shown in Figure 3.2a, the fresh B4 $CsPbBr_3$ QDs supernatant has an absorption band edge at 520 nm with a exciton peak at 516 nm. The exciton peak separates into two peaks at 506 and 523 nm after stored in the N_2 glovebox for 35 days, which implies some $CsPbBr_3$ QDs disassembled to smaller particles and other particles grow to larger particles according to the quantum confinement effect. In the PL spectrum as shown in Figure 3.2b, compared with the fresh $CsPbBr_3$ QDs, the stored $CsPbBr_3$ QDs supernatant has a lower PL intensity, which might be attributed to the slow degradation that can influence the optical properties of $CsPbBr_3$ QDs with the increasing time. Some defects could be formed on QD surfaces during the growth. These defects could also lead to the degradation of QD over time.[14]

3.2 Synthesis of $CsPbBr_3$ QDs with ligands in precursor

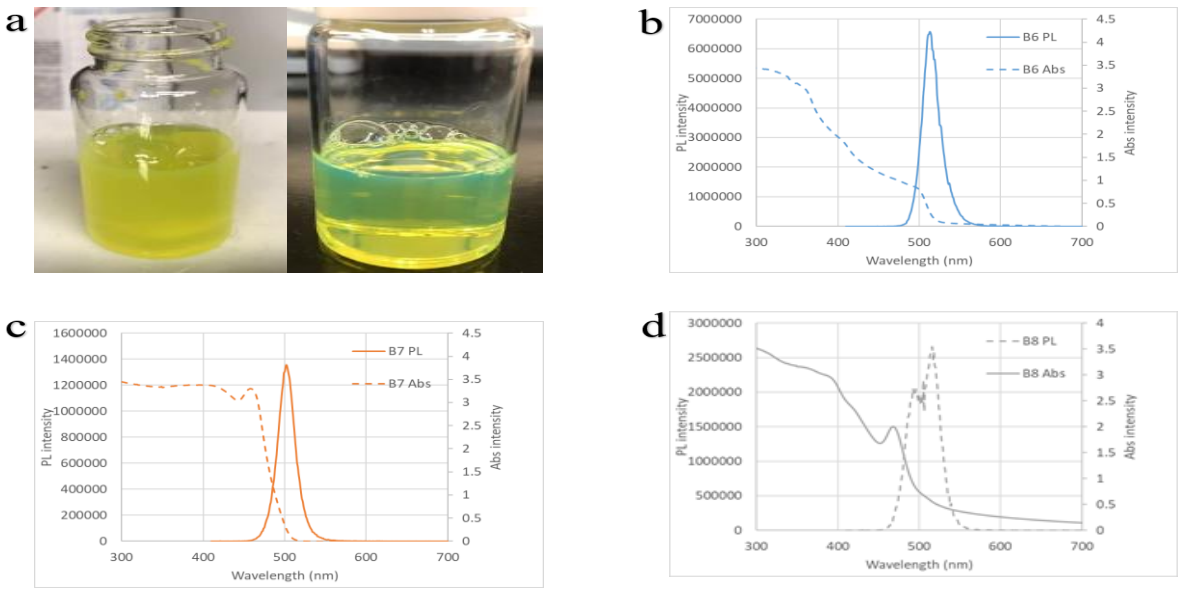

Figure 3. 3 (a) Photographs of as synthesized (left) and supernatant (right) of B7 $CsPbBr_3$ QDs. UV-Vis absorption and PL spectra of (b) B6, (c) B7, and (d) B8 $CsPbBr_3$ QDs. The excitation wavelength is 365 nm for PL.

The colloidal CsPbBr3 QDs were also synthesized via the LARP method with the ligands in precursor and the detailed conditions for different batches are listed in Table 2.2. A mixture of CsBr and PbBr2 was dissolved in DMF in order to form the precursor. Then, OA and OLA ligands were added in the precursor and the mixed precursor solution was gradually added into a vigorously stirred toluene anti-solvent. After this, a yellow-green colloidal solution was formed as shown in Figure 3.3a (left), implying an aggregation process of the precursor into nanoparticles. We set the amount of B6's injected precursor as 1x, the amount of B7's injected precursor as 4x and the amount of B8's injected precursor as 8x. It was also revealed that the crystallization process was controlled by supersaturation, which was initially induced by the solubility change with solvent mixing.[14] The crude colloidal solution was transferred into FEP centrifuge tubes and centrifuged at 4000 rpm for 10 min at room temperature. After that, we obtained the high-quality $CsPbBr_3$ QDs colloidal solution as shown in Figure 3.3a (right). The optical properties of different

batches were further investigated via UV-Vis and PL spectrometers. As shown in Figures 3.3b-d, $CsPbBr_3$ QDs synthesized in batch-6, batch-7 and batch-8 have the absorption band edges at 525, 502 and 515 nm. Compared with batch-7, injecting more or less precursor produced larger size $CsPbBr_3$ QDs, indicating by the redshift of absorption edge. Besides, compared with batch-6 and batch-8, batch-7 shows more $CsPbBr_3$ QDs produced in toluene according to the intensity of UV-Vis spectra. Also as shown in Figure 3.3b-d, PL spectra of batch-6 and batch-7 exhibit sharp emission peaks at 515 and 505 nm, respectively. PL spectrum of batch-8 exhibits two sharp peaks at 496 nm and 514 nm. Compared with other batches, batch-6 shows the better quality of $CsPbBr_3$ QDs according to the intensity of PL, which implies the synthesized $CsPbBr_3$ QDs of batch-6 might have better luminescence quantum yield. The obvious Stokes shift of each batch implies the PL emission originates from excitonic recombination. As shown in Figures 3.3b and c, only one narrow peak exhibits in the PL spectra, implying uniform size and shape $CsPbBr_3$ QDs because the PL peaks depend on the particle size and shape.[15] As shown in Figure 3.3d, there are two PL peaks, implying that QDs with different sizes and shapes could be formed in Batch-8. This might be attributed to the injection of more precursor that leads the growth of $CsPbBr_3$ nanocrystals rather than the formation of new nanocrystals. At much more amount of the precursor, the $CsPbBr_3$ particles get closer and form aggregates of a few micrometers and two dimensional nanoplatelets which is consistent with the previous observation involving excess amounts of the precursor in the literature.[16,17]

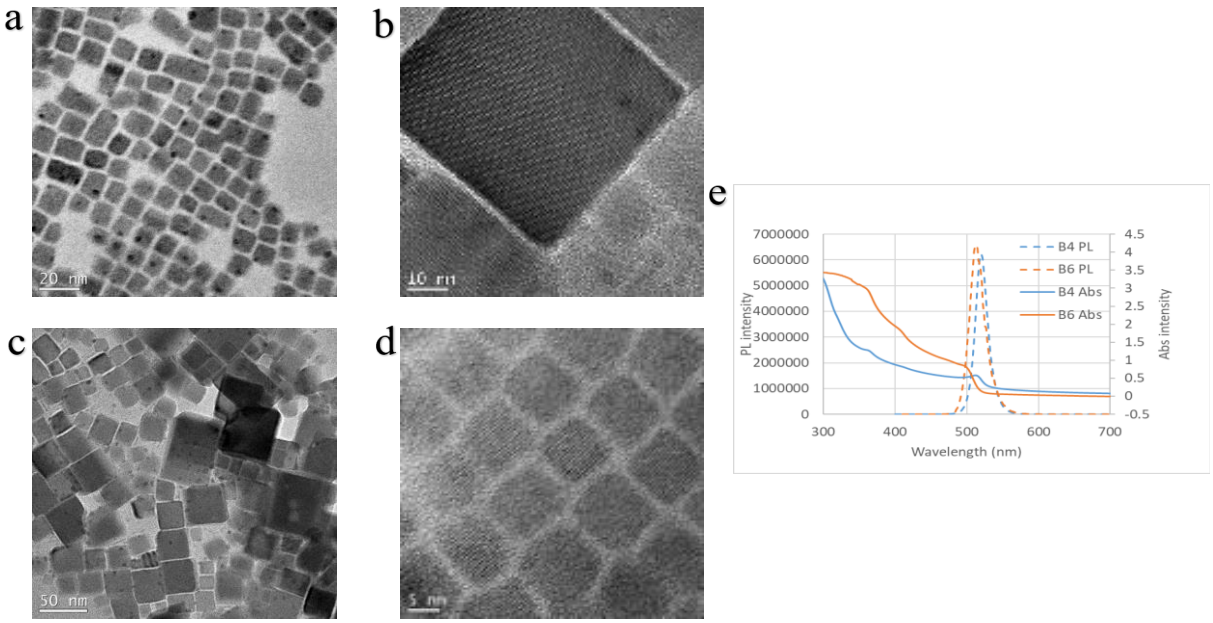

Figure 3. 4. (a, c) TEM and (b, d) high-resolution TEM images of B4 and B6 $CsPbBr_3$ QDs, respectively. (e) UV-Vis absorption and PL spectra of B4 and B6 $CsPbBr_3$ QDs. The excitation light is 365 nm for PL.

The size and shape characteristics of the $CsPbBr_3$ QDs synthesized with the ligands in anti-solvent and in precursor can be clearly seen in the TEM images in Figures 3.4a and c. The QD size of B4 is in the range of 15-50 nm and the size of B6 is in the range of 10-15 nm. The results were obtained by similar synthetic protocol but ligands were in anti-solvent for B4 and in precursor for B6. Synthesis of $CsPbBr_3$ QDs with ligands in precursor obtained much smaller and more uniform particles as shown in Figure 3.4c, implying ligands in precursor would bind more strongly and more easily to surfaces of particles than ligands in anti-solvent because ligands were found to play an important role in determining the shape, size and photoluminescence properties of the QDS as described in the literature.[18] Single crystal structure and crystal lattice planes can be identified clearly in the high-resolution TEM images as shown in Figure 3.4b and d. As evidenced by Figure 3.4e, the UV-Vis absorption spectrum of B4 has a band edge at 512 nm that is red-shift by ~10 nm from that of the B6 and the PL spectrum of B4 has a sharp peak at 520 nm, which is red-shift by

~8 nm from that of the B6. These red-shifts are attributed to the particle size of B4 is bigger than B6 because of the size-dependent quantum confinement effect.[19] Although the amount of $CsPbBr_3$ QDs of B6 might be more than the amount of $CsPbBr_3$ QDs of B4 as shown in UV-Vis spectra, the uneven CsPbBr3 QDs of B4 might have better PLQY compared with B6 according to the same PL intensity with B6 as shown in PL spectra.

3.3 Synthesis of $CsPbBr_3$ QDs with PTB7 or PTB7-Th in toluene as anti-solvent

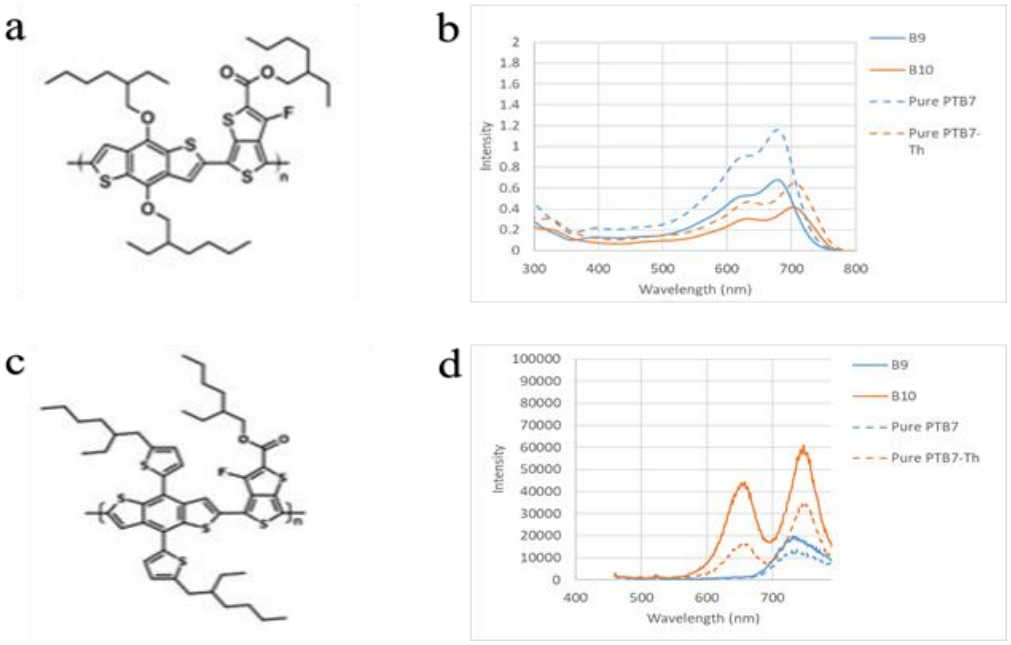

Figure 3.5. (a, c) Molecule structures of PTB7 and PTB7-Th conjugated polymer, respectively. (b, d) UV-Vis absorption and PL spectra of B9, B10, and pure PTB7 and PTB7-Th solution. The excitation light is 400 nm for PL.

Direct synthesis of lead sulfide (PbS) nanocrystals in the conjugated polymer 2-methoxy-5-(2'-ethyl-hexyloxy)-p-phenylene (MEH-PPV) was reported by using a hot injection method.[20] In a standard nanocrystal synthesis, growth control is derived from a combination of electrostatic effects from the surfactant functional groups (e.g. phosphine). MEH-PPV has no charged functional groups that could electrostatically control nanocrystal growth but it can influence the

growth by long polymer chain. The nanocrystals self-assemble, are highly crystalline and are electronically coupled to MEH-PPV according to the PL and TEM spectra. In order to synthesize $CsPbBr_3$ QDs with the presence of conjugated polymer, we adjusted the conventional LARP method by using PTB7 or PTB7-Th conjugated polymer instead of OA and OLA ligands and the detailed experimental conditions are provided in Table 2.3. Molecular structures of two conjugated polymer materials are given in Figure 3.5a and c. A mixture of CsBr and $PbBr_2$ was dissolved in DMF in order to form the precursor. Toluene was used to dissolve PTB7 (0.4 mg/mL) or PTB7-Th (0.4 mg/mL) and also served as anti-solvent for the synthesis of $CsPbBr_3$ QDs with the LARP method. After injecting the precursor into the PTB7 or PTB7-Th solution, we cannot see any obvious color change. After centrifuge using FEP centrifuge tubes at 12000 rpm for 10 min at room temperature, we collected the supernatant for further analysis of its optical properties. As shown in Figures 3.5b and d, there are no obvious differences in the UV-Vis absorption and PL spectra for B9 and pure PTB7 solution, which implies that $CsPbBr_3$ QDs may not form in PTB7 solution. For B10 that was attempted to synthesize $CsPbBr_3$ QDs in PTB7-Th toluene solution, there are also no obvious differences in the UV-Vis absorption and PL spectra for B10 and pure PTB7-Th solution. Further studies are needed to understand the mechanisms of synthesizing nanoparticles directly in the conjugated polymers solutions.

3.4 Photodetectors with F8T2: $CsPbBr_3$ QDs

3.4.1 Photodetectors with BCP as the electron transport layer

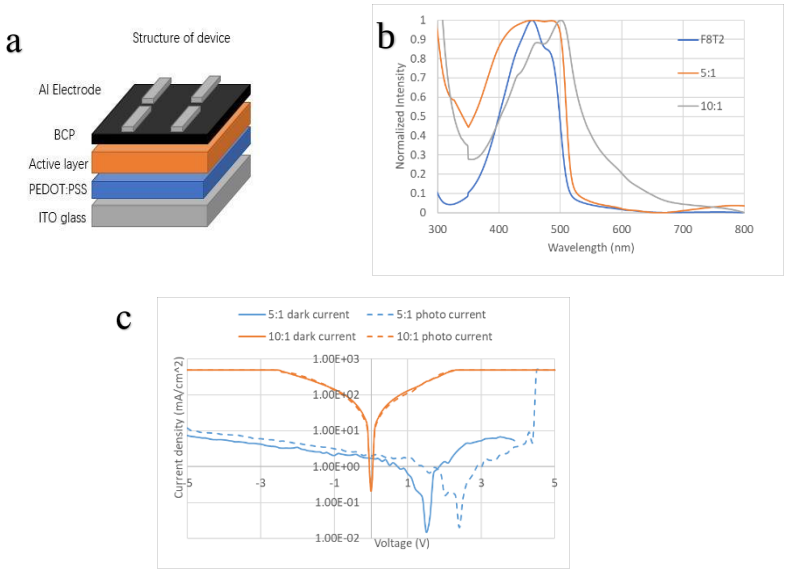

Figure 3.6. (a) Schematics of the device structure. (b) Normalized UV-Vis absorption spectra of F8T2 film (230 nm) and F8T2:$CsPbBr_3$ QDs blend films with 5:1 (183 nm) and 10:1 (260 nm) weight ratios. (c) Dark and 450 nm light illuminated J-V curves.

We fabricated photodetectors with the conventional device structure of ITO/PEDOT:PSS/F8T2:CsPbBr3/BCP/Al (as shown in Figure 3.6a), where ITO and Al are the anode and cathode, respectively, and PEDOT:PSS and BCP are the hole transport layer and electron transport layer, respectively.[21] Low $CsPbBr_3$ content films with F8T2:$CsPbBr_3$ weight ratios of 5:1 and 10:1 were used as the active layer of the devices. The active layers of two devices were using F8T2 (30000 g/mol) at concentration of 25 mg/mL, blended with $CsPbBr_3$ at a low concentration of 5.8 mg/mL, spin coated at 1000 rpm for 30s, and annealed at 80 ℃ for 10 min. In order to investigate the optical properties of active layer film, we tested the UV-Vis spectrum of the film. As shown in Figure 3.6b, the F8T2 thin film has a strong absorption peak at 454 nm and a lower peak at 485 nm, with a sharp cutoff around 500 nm. The absorption spectra of the blended

F8T2 and $CsPbBr_3$ resemble the absorption of a F8T2 thin film with two peaks. The addition of $CsPbBr_3$ QDs make the absorption peak red shift and make the cutoff at 530 nm in the thin film with weight ratio of 5:1 and 630 nm in the thin film with weight ratio of 10:1. The dark and illuminated current density-voltage characteristics for all two devices are shown in Figure 3.6c. The dark currents of two devices are so high that we could not observe obvious difference between dark current and photo current. Compared with the device with weight ratio of 10:1, the device with ratio of 5:1 shows more obvious rectification phenomenon and lower dark current, which implies the weight ratio of active layer might influence performance of device.[22]

3.4.2 Fabricate devices by using LiF as the electron transport layer

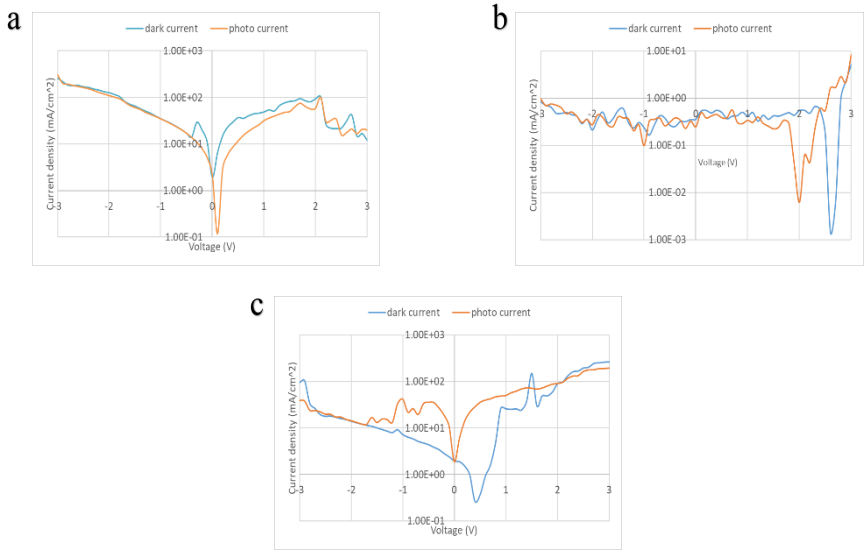

Figure 3.7. (a) Dark and illuminated J-V curves of device with weigh ratio of 100:4. (b) Dark and illuminated J-V curves of device with weight ratio of 1:3. (c) Dark and illuminated J-V curves of device with weight ratio of 1:6. (the illuminated light is 450 nm)

In order to decrease the noise current and dark current, we tried to use the LiF instead of BCP as the electron transport layer with the structure of device as shown in Figure 3.6a and adjust the weight ratio of F8T2:$CsPbBr_3$. The first active layer with F8T2:$CsPbBr_3$ weight ratio of 100:4 was using F8T2 (30000 g/mol) at concentration of 25 mg/mL, blended with $CsPbBr_3$ at a low

concentration of 5.8 mg/mL. The last two active layers with F8T2:$CsPbBr_3$ weight ratios of 1:3 and 1:6 were using F8T2 (30000 g/mol) at concentration of 25 mg/mL, blended with $CsPbBr_3$ at a high concentration of 11.6 mg/mL via concentrate process as described before. Although we used the LiF as the electron transport layer and adjust the weight ratio of F8T2:$CsPbBr_3$, all of three devices are still unstable and have high dark current. According to previous literatures, the high dark current can be attributed to the poor hole/electron blocking ability at the interface between the transport layer and HP material.[23-25] Besides, the poor contact between various transporting layers and solution processed halide perovskite is unavoidable, which is one of the causes of leakage current.

Chapter 4. CONCLUSION

In summary, in this work, we adopted a ligand-assisted reprecipitation (LARP) technique with some modifications to synthesize $CsPbBr_3$ QDs. These $CsPbBr_3$ QDs synthesized by using ligands show excellent crystalline and show different sizes and optical properties under different experimental condition. Compared with the $CsPbBr_3$ QDs synthesized with ligands in anti-solvent, the $CsPbBr_3$ QDs synthesized with ligands in precursor shows more uniform and smaller size. Although we could not synthesis $CsPbBr_3$ QDs with conjugated polymers instead of ligands, the method needs to further research. We have fabricated conventional photodetectors utilizing F8T2:$CsPbBr_3$ blend active layers with different ratios, with an electron transport layer of BCP or LiF. Although all of devices are unstable, we find the weight ratio of F8T2:$CsPbBr_3$ and the interface between transport layer and halide perovskite will influence the stability and dark current of device. In the future, we plan to do more researches about the $CsPbBr_3$ QDs applied on the photodetectors.

REFERENCE

[1] Wells, H. L. U¨ber die Ca¨sium- und Kalium-Bleihalogenide. Z. Anorg. Chemie 1893, 3, 195−210.

[2] J. Shamsi; A. S. Urban; M. Imran; L. Trizio; L. Manna. Metal Halide Perovskite Nanocrystals: Synthesis, Post-Synthesis Modifications, and Their Optical Properties. Chem. Rev. 2019, 119, 3296-3348.

[3] Wang, H. C.; Bao, Z.; Tsai, H. Y.; Tang, A. C.; Liu, R. S. Perovskite Quantum Dots and Their Application in Light-Emitting Diodes. Small 2018, 14, 1702433.

[4] Li, X.; Cao, F.; Yu, D.; Chen, J.; Sun, Z.; Shen, Y.; Zhu, Y.; Wang, L.; Wei, Y.; Wu, Y.; et al. All Inorganic Halide Perovskites Nanosystem: Synthesis, Structural Features Optical Properties and Optoelectronic Applications. Small 2017, 13, 1603996.

[5] Papavassiliou, G. C.; Pagona, G.; Karousis, N.; Mousdis, G. A.; Koutselas, I.; Vassilakopoulou, A. Nanocrystalline/microcrystalline materials based on lead-halide units. J. Mater. Chem. 2012, 22, 8271−8280.

[6] Protesescu, L.; Yakunin, S.; Bodnarchuk, M. I.; Krieg, F.; Caputo, R.; Hendon, C. H.; Yang, R. X.; Walsh, A.; Kovalenko, M. V. Nanocrystals of Cesium Lead Halide Perovskites ($CsPbX_3$, X = Cl, Br, and I): Novel Optoelectronic Materials Showing Bright Emission with Wide Color Gamut. Nano Lett. 2015, 15, 3692−3696.

[7] Li, X.; Wu, Y.; Zhang, S.; Cai, B.; Gu, Y.; Song, J.; Zeng, H. $CsPbX_3$ Quantum Dots for Lighting and Displays: Room-Temperature Synthesis, Photoluminescence Superiorities, Underlying Origins and White Light-Emitting Diodes. Adv. Funct. Mater. 2016, 26, 2435−2445.

[8] Seth, S.; Samanta, A. A Facile Methodology for Engineering the Morphology of $CsPbX_3$ Perovskite Nanocrystals under Ambient Condition. Sci. Rep. 2016, 6, 37693.

[9] Junpeng Zeng; Cuifang Meng; Xiaoming Li; Ye Wu; Shuting Liu; Hai Zhou; Hao Wang; Haibo Zeng. Interfacial-Tunneling-Effect-Enhanced $CsPbBr_3$ Photodetectors Featuring High Detectivity and Stability. Adv. Funct. Mater. 2019, 29, 1904461.

[10] Zhang, F.; Zhong, H.; Chen, C.; Wu, X. G.; Hu, X.; Huang,H.; Han, J.; Zou, B.; Dong, Y. Brightly Luminescent and Color-Tunable Colloidal $CH_3NH_3PbX_3$ (X = Br, I, Cl) Quantum Dots:Potential Alternatives for Display Technology. ACS Nano 2015, 9, 4533−4542.

[11] Lamer, V. K.; Dinegar, R. H. Theory, Production and Mechanism of Formation of Monodispersed Hydrosols. J. Am. Chem. Soc. 1950, 72 (11), 4847−4854.

[12] Zheng, K.; Zhu, Q.; Abdellah, M.; Messing, M. E.; Zhang, W.; Generalov, A.; Niu, Y.; Ribaud, L.; Canton, S. E.; Pullerits, T. Exciton Binding Energy and the Nature of Emissive States in Organometal Halide Perovskites. J. Phys. Chem. Lett. 2015, 6 (15), 2969−2975.

[13] E. Moyen; A. Kanwat; S. Cho; H. Jun; R. Aad; J. Jang. Ligand removal and photo-activation of $CsPbBr_3$ quantum dots for enhanced optoelectronic devices. Nanoscale, 2018, 10, 8591.

[14] X. Du; G. Wu; J. Cheng; H. Dang; K. Ma; Y. Zhang; P. Tan; S. Chen. High-quality $CsPbBr_3$ perovskite nanocrystals for quantum dot light emmiting diodes. RSC Adv, 2017, 7, 10391.

[15] A. Kirakosyan; J. Kim; S. Lee; I. Swathi; S. Yoon; J. Choi. Optical Properties of Colloidal $CH_3NH_3PbBr_3$ Nanocrystals by Controlled Growth of Lateral Dimension. Cryst. Growth Des. 2017, 17, 794-799.

[16] Sichert, J. A.; Tong, Y.; Mutz, N.; Vollmer, M.; Fischer, S.; Milowska, K. Z.; Cortadella, R. G.; Nickel, B.; Cardenas-Daw, C.; Stolarczyk, J. K.; Urban, A. S.; Feldmann, J. Quantum Size Effect in Organometal Halide Perovskite Nanoplatelets. Nano Lett. 2015, 15, 6521−6527.

[17] Tyagi, P.; Arveson, S. M.; Tisdale, W. A. Colloidal Organohalide Perovskite Nanoplatelets Exhibiting Quantum Confinement. J. Phys. Chem. Lett. 2015, 6, 1911−1916.

[18] S. Seth; A. Samanta. A Facile Methodology for Engineering the Morphology of $CsPbX_3$ Perovskite Nanocrystals under Ambient Condition. SCIENTIFIC REPORTS, 6:37693.

[19] A.I. Ekimov; Al.L. Efros; A.A. Onushchenko. Quantum size effect in semiconductors microcrystals. Solid State Communications, volume 56, Issue 11, 921-924.

[20] A. Watt; E. Thomsen; P. Meredith; H. Rubinsztein-Dunlop. A new approach to the synthesis of conjugated polymer-nanocrystal composites for heterojunction optoelectronics. Chem. Commun., 2004, 2334-2335.

[21] M. R. Esopi; M. Calcagno; Q. Yu. Organic Ultraviolet Photodetectors Exhibiting Photomultiplication, Low Dark Current, and High Stability. Adv. Mater. Technol. 2017, 2, 1700025.

[22] M. R. Esopi; E. Zheng; X. Zhang; C. Cai; Q. Yu. Tuning the spectral response of ultraviolet organic–inorganic hybrid photodetectors via charge trapping and charge collection narrowing. Phys. Chem. Chem. Phys. 2018, 20, 11273.

[23] L. Dou; Y. M. Yang; J. You; Z. Hong; W.-H. Chang; G. Li; Y. Yang. Solution-processed hybrid perovskite photodetectors with high detectivity. Nat. Commun. 2014, 5, 5404.

[24] X. Li; D. Yu; F. Cao; Y. Gu; Y. Wei; Y. Wu; J. Song; H. Zeng. Healing All-Inorganic Perovskite Films via Recyclable Dissolution–Recyrstallization for Compact and Smooth Carrier Channels of Optoelectronic Devices with High Stability. Adv. Funct. Mater. 2016, 26, 5903.

[25] X. Dai; Z. Zhang; Y. Jin; Y. Niu; H. Cao; X. Liang; L. Chen; J. Wang; X. Peng. Solution-processed, high-performance light-emitting diodes based on quantum dots. Nature 2014, 515, 96.